https://doi.org/10.5194/tc-2020-135
Preprint. Discussion started: 8 June 2020

The Cryosphere
Discussions
Open Access
EGU

Electron backscatter diffraction (EBSD) based determination of crystallographic preferred orientation (CPO) in warm, coarse-grained ice: a case study, Storglaciären, Sweden

Morgan E. Monz[1], Peter J. Hudleston[1], David J. Prior[2], Zachary Michels[1], Sheng Fan[2], Marianne Negrini[2], Pat J. Langhorne[2] and Chao Qi[3]

[1]Department of Earth and Environmental Sciences, University of Minnesota, Minneapolis, Minnesota, USA
[2]Department of Geology, University of Otago, Dunedin, New Zealand
[3]Key Laboratory of Earth and Planetary Physics, Chinese Academy of Sciences, Beijing, China

Correspondence to: Morgan E. Monz (monzx001@umn.edu)

Abstract. Microstructures provide key insights into understanding the mechanical behavior of ice. Crystallographic preferred orientation (CPO) develops during plastic deformation as ice dynamically recrystallizes, with the dominance of intracrystalline glide on the basal plane. CPO patterns in fine-grained ice have been relatively well characterized and understood in experiments and nature, whereas CPO patterns in "warm" (T > -10ºC), coarse-grained, natural ice remain enigmatic. Previous microstructural studies of coarse-grained ice have been limited to c-axis orientations using light optical measurements. We have developed a new sample preparation technique, by constructing composite sections, to allow us to use electron backscatter diffraction (EBSD) to obtain a representative, bulk CPO on coarse-grained ice. We suggest that a grain sampling bias of large, branching crystals that appear multiple times as island grains in thin section may result in the typical multiple maxima CPOs previously identified in warm, coarse-grained ice that has been subjected to prolonged shear. CPOs combined from multiple samples of highly sheared ice from Storglaciären provide a more comprehensive picture of the microstructure and yield a pronounced cluster of c-axes sub-normal to the shear plane and elongate or split in a plane normal to the shear direction, and a concomitant girdle of a-axes parallel to the shear plane with a maximum perpendicular to the shear direction. This pattern compares well with patterns produced by sub-sampling data sets from experimentally sheared ice at high homologous temperatures up to strains of ~1.5. Shear strains in the margin of Storglaciären are much higher than those in experimental work. At much lower natural strain rates, dynamic recrystallization, particularly grain boundary migration, may have been more effective so that the CPO has been continuously reset and represents a smaller, final fraction of the shear history, rather than the entire finite strain history. A key result of this study is that the multimaxima CPOs in coarse grained ice reported in previous work may be due to limited sample size and a sampling bias stemming from the presence of island grains of a single host that appear several times in a thin section.

1 Introduction

Ice sheets and glaciers play crucial roles in Earth's climate system, and understanding their dynamic behavior is essential for a variety of predictive purposes, including making projections of glacier and ice sheet discharge and sea level rise (e.g. Bindschadler et al., 2013; Faria et al., 2014b; Dutton et al., 2015; Golledge et al., 2015; Bamber et al., 2019). In addition, glacial ice is a monomineralic rock that deforms at high-homologous

https://doi.org/10.5194/tc-2020-135
Preprint. Discussion started: 8 June 2020

temperatures as ice flows, and glaciers represent natural tectonic systems that undergo the equivalent of regional high-grade metamorphism under known driving forces (Hambrey and Milnes, 1977; Van der Veen and Whillans, 1994). Similar to rocks in active orogens, flowing glacial ice develops both structures and CPOs that reflect the conditions and kinematics of deformation. Studying the internal structure of glaciers on the crystal scale provides key insights into ice mechanics, and aids in the understanding of tectonic processes (Hambrey and Milnes, 1977; Hooke and Hudleston, 1978; Faria et al., 2014b; Wilson et al., 2014; Hudleston 2015).

Quantifying flow behavior of ice under natural conditions is essential for the accurate incorporation of glacier flow into climate models and for using ice as an analog for high temperature deformation of crustal and mantle rocks (Faria et al., 2014b). Glaciers move by two gravity-driven processes: (1) frictional sliding (including deformation of underlying sediments) of the ice mass over the underlying rock surface (e.g. Flowers, 2010 and references therein), and (2) slow, continuous creep (flow) within the ice mass itself (e.g. Glen, 1955; Alley, 1992; Budd and Jacka, 1989; Cuffey and Paterson, 2010). Creep is governed by thermally-dependent, micro-scale deformation processes, and therefore participates in important thermo-mechanical feedbacks in the Earth's cryosphere, atmosphere and oceans. This is especially important because of the highly non-linear dependence of strain rate on stress (Glen, 1955; Budd and Jacka, 1989; Bons et al., 2018)

Terrestrial glaciers, ice sheets and ice shelves comprise crystals of hexagonal ice (Ih, Fig. 1a; Pauling, 1935; Faria et al., 2014b). As ice dynamically recrystallizes during flow, anisotropy in the form of a crystallographic fabric or crystallographic preferred orientation (CPO) develops due to a dominance of intracrystalline glide on the basal plane (Weertman, 1983; Duval et al., 1983; Faria et al., 2014b). Similar to other crystalline materials, CPO development modifies the internal flow strength (e.g. Wenk and Christie, 1991); and thus documenting natural ice CPOs provides insight into the large-scale flow rates of glaciers and ice sheets (e.g. Faria et al., 2014b). The CPO of ice is commonly represented by the preferred orientation of c-axes. This is useful because the c-axis of an ice crystal is normal to the basal plane (Fig. 1a), and glide on this plane dominates deformation (Duval et al., 1983). However, the orientations of a-axes are needed to fully characterize the orientation of ice crystals, and better understand deformation mechanisms.

Coarse-grained (highly variable, but typically greater than 20mm) ice is common at the base of ice sheets and in warm (T > -10ºC) glaciers. Work on coarse-grained ice is especially important because basal ice in ice sheets may accommodate much more of the ice flow than the colder ice higher up the ice column (e.g. Rignot and Mouginot, 2012; MacGregor et al., 2016). Previous studies on coarse-grained ice have likely only measured partial CPOs, typically by optical methods (c-axes only), and identified apparent multiple-maxima patterns defined by isolated clusters of c-axes (Fig. 1b; e.g. Rigsby, 1951; Kamb, 1959; Jonsson, 1970). However, these multiple-maxima patterns are incompletely understood and defined in part because there has been no practical method for measuring the a-axes associated with such patterns. Measuring the a-axes means that we can tell whether two grains (in a 2D slice) with the same c-axis orientation also have the same a-axes and may be two slices through the same grain in 3D. Work on coarse-grained ice has been limited because methods used to measure CPOs are restricted to section sizes of 100mm x 100mm or smaller, which results in there being an insufficient number of grains needed to clearly define the CPO pattern.

We aim to (1) fully quantify the CPO patterns (c- and a-axes) associated with warm, coarse-grained ice using cryo-electron backscatter diffraction (cryo-EBSD), (2) understand how and why the apparent multimaxima CPO patterns develop, and (3) interrogate the relationships among multimaxima CPO patterns and

https://doi.org/10.5194/tc-2020-135
Preprint. Discussion started: 8 June 2020


The Cryosphere Discussions
Open Access
EGU

local deformation conditions in the ice. To address these objectives, we combine results from fieldwork and laboratory analyses on Storglaciären, a small valley glacier in northern Sweden. Fieldwork included detailed mapping of structural features to provide a large-scale kinematic framework for our lab-based, microstructural part of the study. Importantly, in the lab we developed a new sample preparation method to allow us to measure a representative volume and number of grains necessary for robust CPO characterization in coarse-grained ice using cryo-EBSD.

2 Previous work

Much of the pre-existing research on CPO development in natural ice has been done on ice cores from Antarctica and Greenland, and this has been nicely synthesized by Faria et al. (2014a). Schytt (1958) produced the first microstructural study of deep polar ice from the ice core extracted from the Norwegian-British-Swedish-Antarctic Expedition of 1949-1952. Many studies of ice cores have been subsequently undertaken, on both Antarctica (Gow and Williamson, 1976; Lipenkov et al., 1989; EPICA community members, 2004; Seddik et al., 2008; Durand et al., 2009; Weikusat et al., 2009b; Azuma et al., 1999, 2000; Weikusat et al., 2017) and Greenland (Herron and Langway, 1982; Herron et al., 1985; Langway et al., 1988; Thorsteinsson, 1997; Gow et al., 1997; Wang et al., 2002; Svensson et al., 2003b; Montagnat et al., 2014). Studying microstructures in ice sheets offers the advantages of examining an extensive record of ice deforming under relatively simple kinematic conditions. As a result, CPOs in ice caps have been well defined and interpreted from ice cores.

There are two typical end member c-axis CPO patterns that have been identified in experimental work. At warm temperatures and lower strain rates under uniaxial compression, the c-axes define an open cone shape or small circle girdle at 30-60^{o} about the axis of compression on a CPO plot (Fig. 1c; e.g. Jacka and Maccagnan, 1984; Alley, 1988; Budd and Jacka, 1989; Jacka and Jun, 2000; Treverrow et al., 2012; Piazolo et al., 2013; Montagnat et al., 2015; Vaughan et al., 2017; Qi et al., 2017). Whether this CPO occurs in nature is less clear. Possible examples are described at the center of ice domes (e.g. Hooke and Hudleston, 1981; Lile et al., 1984; Gow and Meese, 2007). Representations of open cone CPOs do not appear in syntheses of polar bore holes (Faria et al., 2014a). Under simple shear conditions, the basal planes of ice crystals dominantly align with the shear plane, and the c-axes form an asymmetric bimodal distribution with both a strong maximum perpendicular to the shear plane and a weaker secondary cluster offset at an angle antithetic to the rotation associated with the shear direction (Fig. 1c). The angle between the two clusters varies with shear strain, and the weaker cluster ultimately disappears with increasing strain leaving a strong single maximum pattern normal to the shear plane (Fig. 1d; e.g. Duval, 1981; Bouchez and Duval 1982; Budd and Jacka, 1989; Budd et al., 2013; Qi et al., 2019; Journaux et al., 2019). This dual maxima pattern of CPO development under simple shear has been described in nature (Hudleston, 1977a; Jackson and Kamb, 1997). It is probable that the strong single vertical maxima seen in many ice cores from Antarctica and Greenland are associated with zones of sub-horizontal simple shear (Faria, 2014).

An enigmatic CPO pattern can develop in valley glaciers and deep in ice sheets in coarser grained ice that has undergone significant recrystallization. This pattern is always associated with warmer ($T > -10$ºC) conditions and an increase in grain size, and is characterized by 3-4 maxima (sometimes with submaxima), arranged around an axis that is vertical in ice sheets (Gow and Williamson, 1976; Thwaites et al., 1984;

https://doi.org/10.5194/tc-2020-135
Preprint. Discussion started: 8 June 2020

Goossens et al., 2016), and perpendicular to foliation in valley glaciers (Fig. 1b, Fig. 2; Kamb, 1959; Allen, 1960; Budd, 1972; Jonsson, 1970). In most cases, given the coarse grain size (Fig. 2a), the number of grains measured per thin section is small, usually no more than ~100. This may or may not be enough to reveal a mechanically significant CPO pattern (Fig. 2b; Rigsby, 1960). By contrast, CPO plots produced for other deformed crystalline materials typically include data from several hundred unique grains/crystals, which can usually be collected from a single sample section. This would be difficult or impossible to accomplish with coarse-grained ice.

Previous studies on valley glaciers done by Rigsby (1951) on Emmons glacier, Kamb, (1959) on Blue Glacier, and Jonsson (1970) on Isfallsglaciären used light optical measurements to delineate a CPO characterized by a multimaxima pattern of the type described above, but were limited to measuring c-axis orientations. Such studies used a Rigsby universal stage to individually orient c-axes (Langway, 1958), and they demonstrated a relationship of the overall c-axis CPO to other structural elements, with the pole to foliation typically located centrally among the maxima (Jonsson, 1970).

Possible analogues to the multimaxima CPOs found in nature have been produced in experiments by Steinemann (1958) and Duval (1981), in both cases done at temperatures near the melting point and under torsion-compression conditions. The maxima developed at high angles to the shear plane. It should be noted however, that the grain size in the experiments is much smaller than in natural ice with these CPOs.

Ice with the multi maxima CPO in valley glaciers (Rigsby, 1951; Kamb, 1959; Jonsson, 1970) and deep in ice sheets (Gow and Williamson, 1976) is comprised of large, branched crystals that lack undulose extinction and have irregular, lobate grain boundaries (Fig. 2a; Fig. 3). The branching nature of these crystals may result in sectioning artifacts that lead to apparent "island grains"—branches of the same grain appearing multiple times throughout one 2D thin section (Fig. 3: e.g. as observed by Dempsey and Langhorne (2012) in sea ice). Without a complete crystal orientation – one which includes ice a-axes – it is difficult to confirm the existence of such island grains and determine their effect of the characterization of a representative CPO.

Earlier studies made efforts to quantify an angular relationship between clusters of c-axes, but no consistent relationship could be found, and a mechanism that produces such a pattern – with regular angular relationships or otherwise – has not been established, although it has been proposed that the multimaxima pattern may be the result of twinning (Matsuda and Wakahama, 1978) alteration of a preexisting CPO (Kamb, 1959), or somehow related to the kinematics of combined shear and compression (Duval, 1981).

We argue that no previously employed method has been able to determine a representative CPO for glacial ice consisting of coarse, branching crystals. Optical studies using the Rigsby stage, which accommodates 100mm x 100mm thin sections, are time consuming, and are limited not only by incomplete crystal orientations, but also by data resolution. Automatic ice texture analyzers (AITA), which can also accommodate larger grain sizes, use an image-analysis technique under cross-polarized light to determine c-axes (Russell-Head and Wilson, 2001; Wilen et al., 2003). AITA analyses are attractive for speed and data resolution, but are also limited by incomplete crystal orientations (Russell-Head and Wilson, 2001). Three methods: etching (Matsuda 1979; Matsuda and Wakahama 1978), Laue diffraction (Miyamoto et al 2011; Weikusat et al 2011), and EBSD (Dingley, 1984; Prior et al., 1999) enable the measurement of full crystallographic orientations in ice. Etching is time intensive and the results are of low angular resolution. The other two methods produce results of high resolution.

https://doi.org/10.5194/tc-2020-135
Preprint. Discussion started: 8 June 2020

Cryo-EBSD as a technique was first applied to ice in 2004 (Iliescu et al 2004), and modern cryo-EBSD methods enable routine work on water ice (Prior et al 2015). CPOs derived from EBSD datasets include a-axis orientations and provide a comprehensive view of ice microstructure that can improve our knowledge of the CPO and its relation to ice flow mechanisms on the grain scale. In addition, the speed, angular precision, and spatial resolution attainable with modern EBSD systems offer major advantages over optical methods. However, until now, EBSD has not been applied to warm, coarse-grained ice because a sample of maximum size for analysis (60mm x 40mm: Prior et al., 2015; Wongpan et al., 2018) will only contain a few grains. The procedure we propose in this paper addresses this limitation.

3 Geologic Setting

Storglaciären is a small polythermal valley glacier located in the Tarfala Valley in northern Sweden (Fig. 4). The glacier is 3.2km long, extending in an E-W direction, with a total surface area of 3.1km^2. A cold surface layer (annual mean of -4.0ºC) (Hooke et al., 1983a; Holmlund and Eriksson, 1989; Pettersson et al., 2007) of variable thickness (20-60m) (Holmlund and Eriksson, 1989; Holmlund et al., 1996; Pettersson et al., 2003), and a cold-based margin and terminus (annual mean of -4.0ºC) (Holmlund et al., 1996; Pettersson, 2007), characterize the ablation zone of Storglaciären (Holmlund et al., 1996b). The thermal regime influences glacier dynamics; the center of the glacier undergoes basal sliding, but the margins and terminus are frozen to the overlying and marginal rock (Holmlund et al., 1996), causing most of the deformation in these areas to be a result of creep (Petterson et al., 2007). Storglaciären was chosen because: (1) a compilation of preexisting information on surface velocities and seasonal changes gathered over many years exists to provide background for the study; (2) the multimaxima pattern has been observed optically in strongly sheared marginal and basal ice (Fig. 2), and (3) because it is comparatively easy to access.

Primary stratification is easily identified above the equilibrium line on the glacier as gently undulating layers roughly parallel to the ice surface.. The ice in Storglaciären undergoes horizontal compression and shortening as it enters the valley from the accumulation cirques, and this amplifies the slight undulations in primary stratification, causing upright, similar folds (Ramsay, 1967) near the margins of the valley (walls) where shearing, which combines with shortening, is most intense. Folds range from centimeter to meter amplitude, and generally have axial surfaces that are vertical near the margins and contain the flow direction. They are associated with an axial planar foliation and have hinges that plunge gently west, away from the flow direction. Foliation develops from pre-existing stratification, veins and fracture traces where shear is most intense (e.g. Hambrey, 1975; Roberson, 2008; Jennings et al., 2014), and is defined by variations in crystal size, shape and bubble concentration and distribution (e.g. Allen et al., 1960; Hambrey, 1975; Hambrey and Milnes, 1977; Hooke and Hudleston, 1978). Foliation tends to become perpendicular to the maximum shortening direction, and thus rotate with progressive shear towards parallelism with the flow direction along the glacier margins (Fig. 4; Ragan, 1969), reflecting cumulative strain (Hambrey and Milnes, 1977; Hooke and Hudleston, 1978; Hambrey et al., 1980; Hudleston, 2015).

4 Methods

https://doi.org/10.5194/tc-2020-135
Preprint. Discussion started: 8 June 2020

4.1 Field Work

Detailed mapping in 2016 and 2018 on the surface of the glacier provides the structural framework for this study. Data collection was focused on multiple transects across the glacier in the ablation zone. Relevant data, presented in Figure 4, highlight the relationship of the structures to one another and the known kinematics.

We collected samples from eight areas of intense deformation in the ablation zone during the 2018 field season. For the purposes of this paper, we are focusing on three samples from the intensely sheared southern margin (SG23, SG27, and SG28) (Fig. 4). We excavated 10-20cm of surficial ice before sampling to avoid a layer of solar-damaged, recrystallized ice. Damaged ice was broken up using an ice axe and removed with a shovel. Blocks of ice were removed from the glacier using a small chainsaw. Each sample was ~15x15x30cm, oriented such that the top of the block was parallel to the glacier surface, and the long axis was N-S, perpendicular to the flow direction. The shear plane, used to define the kinematic reference frame for subsequent microstructural analyses, is assumed to be parallel to the foliation. Samples were immediately shaded with a tarp upon removal to avoid solar damage, then labelled and insulated with ice and jackets to be transported off the glacier. We trimmed samples with a band saw in a cold room at the University of Stockholm, Sweden, and marked the top north edge with a notch. We transported these samples to the University of Otago, New Zealand, in doubly insulated Coleman Xtreme 48L wheeled coolers to be stored in a biohazard freezer set to -31ºC. Samples remained below -20ºC for the entire transport pathway.

4.2 Sample preparation

We prepared samples for microstructural analysis in a cold room (-20ºC) at the University of Otago. To prepare coarse-grained, natural polycrystalline samples for EBSD mapping, we developed a novel composite sample preparation method to maximize the number of grains collected and minimize the number of repeated grains, in order to obtain a representative CPO. We made at least two composite sections for imaging from each of the eight samples, totalling 18 composite sections.

The procedure is highlighted in figure 5. We initially cut each sample block into three 5cm thick slabs perpendicular to the foliation. We then divided each slab into rods, spaced by 5cm, perpendicular to the flow direction and to the foliation. These rods were cut such that they were staggered between sequential slabs, and a series of ~2mm thick slices were cut off of the bottom or top of each rod (easiest to divide each rod into equally spaced cubes before cutting slices due to the delicacy of individual slices). Each slice was labelled, oriented, and stacked sequentially between two wooden blocks within a clamp to hold loose slices together before being cemented. We wrapped wet paper towels around the compiled stack to adhere the slices into a coherent block, ~3.6x5x5 cm. We then cut these blocks in half to generate a flat composite surface, labelled each half, and returned one to storage for future use. We mounted sections on 4x6cm copper and aluminium ingots in the cold room using the freeze-on technique outlined by Craw et al. (2018) and, to ensure secureness, used thin slices of wet paper towels around the edges in contact with the ingot. The exposed surface was then flattened and polished using progressively finer sand paper and then cooled slowly to ~ -90ºC before being inserted into the SEM.

https://doi.org/10.5194/tc-2020-135
Preprint. Discussion started: 8 June 2020

Whole sections of certain areas of the original blocks were prepared for examination, to mitigate loss of information on internal structure due to the small slices for the composite sections. Slabs cut perpendicular to foliation (first step in composite preparation) were polished using progressively finer sandpaper and allowed to sublimate overnight, then illuminated using low angle light, which revealed grains intersecting the surface. Areas of interest in these slabs were targeted for whole section analysis. At least two whole sections were taken from each sample.

4.3 Orientation data collection

A Zeiss Sigma variable pressure field-emission-gun Scanning Electron Microscope (SEM) fitted with a Nordlys EBSD camera from Oxford Instruments was used for EBSD analyses. The instrument is fitted with a custom-built cryo-stage that is continuously cooled by liquid nitrogen from an external dewar via a copper braid connection (Prior et al., 2015). The stage is cooled below -100ºC prior to sample insertion. During the transfer process, the sample did not exceed -80ºC. Once the stage cooled back down to -100ºC, we vented the SEM chamber, allowing the stage temperature to rise to -75ºC, inducing a sublimation cycle outlined by Prior et al. (2015) to remove any residual frost from the sample surface before imaging.

We collected full cross-sectional orientation maps of whole sections (e.g. Fig. 6a,b) and composite sections (e.g. Fig. 7a) at a 50µm step size in order to balance data resolution with such a coarse grain size. SEM settings for EBSD acquisition were a stage temperature of ~-90ºC, a chamber pressure of 3-5Pa, an accelerating voltage of 30kV, a beam current of ~60-70nA, and a sample tilt of 70º. EBSD data were collected using the Aztec Software from Oxford Instruments and exported into Oxford- HKL Channel 5. We used EBSDinterp 1.0, a graphic user interface based MATLAB® program developed by Pearce (2015) to reduce noise and interpolate nonindexed EBSD data points using band contrast variations. Noise reduced data were then processed using MTEX, a texture analysis toolbox for MATLAB® (Bachmann et al., 2010), to determine full crystallographic orientations (CPOs), intergranular misorientations and grain boundaries (Mainprice et al., 2015). The overall CPO in our samples is best represented using one-point-per-grain plots rather than all-pixel orientation plots due to the area bias introduced by larger grains in a small sample size. The kinematic reference frame used for plotting CPO is shown in figure 4.

5 Results

5.1 Field Work

Orientation measurements of bedding and foliation are consistent with previous observations on Storglaciären and other valley glaciers. Bedding is difficult to distinguish from foliation at the margins of Storglaciären, but more obviously recognizable in the center of the glacier. Although locally variable due to folding, in the center of the ablation zone, bedding generally dips shallowly west. Along the margins, the foliation is subvertical, dipping steeply inwards towards the center of the glacier (Fig. 4). In the center towards the front of the glacier, the foliation becomes progressively shallower and dips shallowly up glacier where sheared basal ice is closer to the surface (Fig. 4). The combination of transformed stratification and foliation in

https://doi.org/10.5194/tc-2020-135
Preprint. Discussion started: 8 June 2020

the ablation zone forms a series of arcs on the surface reflecting in three dimensions an overall nested spoon arrangement, opening up glacier, much as described by Kamb (1959) for the Blue Glacier.

5.2 Microstructure

Grains are locally variable in size, ranging from 1mm to >90mm, and shape, and have no apparent consistent shape preferred orientation (SPO). Air bubbles exist as a secondary phase and are found both within grains and on grain boundaries (Figs. 2a and 6a,b). Broadly, there is an inverse correlation between bubble concentration and grain size, and also between bubble concentration and grain boundary smoothness.

5.2.1 Whole Section

The size of an individual whole-section is determined by the technique used for the analysis. For U-stage work it is 100mm x 100mm, whereas for EBSD work it is 40mm x 60mm. Neither section size is large enough to clearly measure the coarse crystal size, but such sections capture the complexity of grain boundaries and crystal shapes. Larger crystals have lobate-cuspate boundaries (Fig. 2a; Fig. 6a,b), and many grains are larger than the size of the thin section. Many larger grains within one measured section have the same color in thin section under cross-polarized light and are shown to have the same crystallographic orientations by EBSD data, with near identical c-axis and a-axis orientations (Fig. 2; Fig. 6,b,c).

Misorientation profiles A-A' (Fig. 6a) and B-B' (Fig. 6b) show that the orientation gradient across individual grains is low. The pixel-to-pixel scatter, mostly less than ±0.5º is typical of the angular error for fast EBSD acquisition (Prior et al., 1999). Profile A-A' shows an abrupt change of about 4º across a subgrain boundary, and no distortion within the grain or subgrain. In nine whole sections analyzed for this study, ~15% of grains contain subgrain boundaries, with misorientations ranging between 2.5º and 5.5º (e.g. Fig. 6a). Profile B-B' shows a grain that has no internal distortion, and profile C-C' shows an orientation change of about 2.5º across ~20mm. The statistics of misorientation between every pixel and the average orientation for that grain (Fig 6e) shows that 99% of these misorientations are below 2.5º. There is very little orientation spread, a measure of lattice distortion in the grains in this and all of the other sections shown.

5.2.2 Composites

Several c-axis maxima clustered around the normal to the shear plane are present in individual samples and this is largely independent of whether we plot all measured pixel orientations or one-point-per-grain orientations (Fig. 7b,c,d). The maxima in the all-pixel diagrams (Fig. 7b) have different relative intensities compared to those in the one-point-per grain CPO plots (Fig. 7c,d), reflecting the increased weight given to the larger grains in the per pixel data. In either case, many c-axes within an individual cluster are only separated by 2-3 degrees. These slight misorientations are likely due to small misalignments of individual slices in the composite section that occurred during the sample preparation process. The a-axes define a diffuse girdle, parallel to sub-parallel with the shear plane, containing three distinct clusters (Fig. 7e). Each cluster is elongate towards the pole to foliation.

https://doi.org/10.5194/tc-2020-135
Preprint. Discussion started: 8 June 2020

When composites SG23, SG27 and SG28, which are in the same kinematic reference frame, are individually plotted as one point per grain, and these results are combined on one CPO plot, the multimaxima nature of the pattern diminishes (Fig. 8). The composite pattern has one c-axis maximum perpendicular to the shear plane, that is elongate or split in a plane normal to the shear direction, and an a-axis girdle parallel with the shear plane with a concentration of a-axes perpendicular to the shear direction (parallel to the inferred vorticity axis of flow). Two weak c-axis sub-maxima are offset from the main maximum in a plane perpendicular to the vorticity axis: the more distinct one ~30º synthetic to the shear direction and the less distinct one ~50º antithetic to the shear direction (Fig. 8).

6 Discussion

6.1 Whole sections

EBSD maps of whole sections confirm that island grains are likely part of the same larger grain (Fig. 6a,b). Individual grains within a two-dimensional surface that have exactly the same orientation or a slight misorientation are likely branching segments of the same grain, or subgrains of the larger grain in three dimensions (Fig. 3; Fig. 6b,c). Even small (30mm x 50mm) 2D sections can contain 3-5 island grains that have the same orientation (Fig. 6b,c). By appearing several times in the same section, some of the larger crystals likely amplify individual maxima within the overall CPO pattern typically identified in warm, coarse-grained ice. This may particularly be the case in studies that only use ~100 or fewer grains to identify a c-axis pattern, because if 10-15 islands comprising the same grain were measured as separate grains, that would automatically lead to a c-axis maximum due to that grain.

Whole section analyses also allowed us to better understand the deformation mechanisms. While some subgrains are present in the suite of whole sections analyzed, most crystals show little evidence of significant lattice distortion. Individual grains are relatively strain free (Fig. 6e). A lack of intragranular distortion, combined with the presence of lobate-cuspate grain boundaries suggests that recrystallization in these samples is dominated by grain boundary migration (Urai et al., 1986). These interpretations are consistent with those in microstructural studies of experimentally deformed ice at high temperatures (e.g. Kamb, 1972; Montagnat et al., 2015; Vaughan et al., 2017; Journaux et al., 2019), and natural ice samples deformed at relatively high temperature (Duval and Castelnau, 1995).

6.2 Composite sections

c-axis patterns for *individual* samples appear to represent typical multimaxima CPO patterns of the kind that have previously been identified in warm, coarse-grained ice (Fig. 7b,c), with 2-3 strong maxima and 1-2 weaker maxima all centered about the pole to foliation. However, on CPO plots for the composite sections from a single sample, individual points within clusters of one-point-per-grain c-axes are only separated by 2-3 degrees, and we interpret the small angular difference as most likely due to branched grains appearing multiple times throughout the sample section, consistent with observations made on whole sections. The small 2-3 degree misorientations of individual c-axes within a cluster are likely due to slight rotation of slices that occurred

https://doi.org/10.5194/tc-2020-135
Preprint. Discussion started: 8 June 2020

during the sample preparation process. As such, we propose that multimaxima patterns such as those described in previous studies may be an *apparent* result caused by grain sampling bias, with some samples containing fewer than 30 *unique grains* within a set of 100 apparent grains (i.e. the case assuming no multiple counting). Thus, even for the composite samples, the data may not truly provide a representative one-point-per-grain CPO.

365

6.3 Comparison with Experimental Results

We compare our CPOs from natural ice to experimentally obtained CPOs from two warm temperature (-5ºC) direct shear experiments done by Qi et al. (2019), at relatively low (γ=0.62) and high (γ=1.5) strains.
370 Except for grain size, we interpret microstructures in the ice from Qi et al. (2019) to be similar to those in our samples from Storglaciären (including c- and a-axis CPOs) and to other examples (including c-axis only CPOs) of warm, natural ice (Rigsby, 1951; Kamb, 1959; Jonsson, 1971). Individual grains from these "warm" experiments done by Qi et al. (2019) are characterized by amoeboidal shapes and lobate boundaries, and portray little to no shape preferred orientation in the two dimensional plane. A major advantage of using the Qi et al.
375 (2019) dataset for our comparison is that it comprises hundreds more grains than can be measured in a single sample of coarse-grained glacial ice – even with using the novel composite-section sampling techniques addressed in this paper. Given the similarity in grain-shape characteristics and deformation temperature, and owing to the greater number of analyzed crystal orientations, we argue that CPO patterns from the Qi et al. (2019) samples represent an excellent analogue for crystallographic texture evolution of ice along the margins of
380 Storglaciären.

Orientation data from Qi et al. (2019) show well-defined CPO patterns with a two-cluster c-axis pattern: a strong c-axis maximum perpendicular to the shear plane, and a c-axis sub-maximum rotated from the dominant maximum 45º-70º in a direction antithetic to the shear induced rotation (Fig. 9). The angle between the strong maximum and sub-maximum decreases with increasing shear strain. Clusters of c-axes are somewhat elongate
385 in a plane normal to the shear direction. This elongation is clear in many previous studies (e.g. Kamb, 1972; Duval, 1981; Bouchez and Duval, 1982, Li et al., 2000; Qi et al., 2019). Kamb (1972), and Budd et al. (2013) suggest that this may be due to compression perpendicular to the shear plane during deformation based on experiments that allow compression in addition to shear or torsion. However, Bouchez and Duval (1982), Li et al. (2000) and Journaux et al. (2019) observed these elongate CPOs in torsion experiments using fixed platens,
390 so compression could not have been a factor in these cases.

The a-axes in both the low- and high-strain experiments of Qi et al. (2019) define a girdle parallel with the shear plane (Fig. 9). In the lower-strain experiments the a-axes cluster mostly perpendicular to the shear direction (parallel to the vorticity axis), whereas in the higher-strain experiments they mostly cluster parallel with the shear direction (Fig. 9). This change in a-axis maximum from normal to shear to parallel to shear with
395 increasing strain is also observed by Journaux et al. (2019).

In an attempt to mimic a possible grain sampling bias similar to that which we propose when dealing with warm coarse-grained ice, we randomly resampled subsets of 50 grains – allowing for random duplicates in the resampling (thus one grain may appear more than once in the resampling) – from the two warm experiments by Qi et al. (2019) at low and high strains and compared these to the stacked suite of natural samples in the same
400 kinematic reference frame (Fig. 9). Subsets of the experimental data produce patterns that are more-diffuse and

https://doi.org/10.5194/tc-2020-135
Preprint. Discussion started: 8 June 2020

patchy than those for the full dataset and are broadly similar to patterns observed in natural coarse-grained ice. Importantly, the Qi et al. (2019) study does not suffer from grain sampling biases common to CPO characterization in warm glacial ice, due to the significantly finer and more consistent grain size (Fig. 9). Compared to the experimental results, the main c-axis maxima in the stacked data from our glacial ice samples (Fig. 8) are more elongate or "pulled apart" than those in the subsampled experimental data, and the girdle of a-axes is broader, with a cluster perpendicular to the shear direction, similar to the pattern observed in the lower strain experiments (Fig. 9). The more distinct c-axis sub-maximum in our combined data (Fig. 8) is offset from the main maximum in a synthetic sense with respect to the shear direction, rather than an antithetic sense as might be expected from the experimental data (Fig. 9). However, the less distinct sub-maximum, offset in the antithetic sense ~50º from the main maximum, is consistent with the secondary maximum in the experiments.

We interpret these results to mean that the grain sampling bias issue was not entirely resolved by making composite sections, due to the very large grain size with interlocking shapes that still have not been entirely characterized. However, the overall similarity between the stacked data from composite sections from the three samples in the same kinematic reference (Fig. 8) to the CPO pattern presented by Qi et al. (2019) for fine-grained ice that has undergone low shear strains at high homologous temperature (Fig. 9, PIL91) suggest that the operative deformation mechanisms are similar.

It is important to note that we do not know the exact deformational history experienced by the ice in our natural samples, but the recent part of that history corresponds most closely to simple shear parallel to the ice margin. An additional similarity between the experiments (Qi et al., 2019) and the conditions of deformation experienced by our samples is that there is a component of compression, which for our natural samples is perpendicular to the margins of the glacier, associated with the narrowing of the valley in the direction of flow (Fig. 10a). Thus our samples may represent similar kinematics to those in the experiments conducted by Duval (1981) and Budd et al. (2013) that involved simple shear combined with compression normal to the shear plane (Fig. 10b).

Hudleston (2015) calculated the shear strain required to rotate fractures towards parallelism with the flow direction along the margins of Storglaciären, and this indicated that the shear strain where we collected ice samples for our study is greater than 2. This estimate exceeds the strain of the "high-strain" experiments done by Qi et al. (2019) and we might therefore expect our data to best match the "high-strain" experimental data. However, the a-axis pattern of our samples best matches the pattern for the "low-strain" experiments. One likely reason for this comes from considering strain rate. In the experiments, shear strain rate was ~10^{-4} s^{-1} whereas in natural ice along the south margin of Storglaciären, strain rate calculated from velocity measurements (Hooke et al., 1983b; Hooke et al., 1989) and modeling (Hanson, 1995) is ~10^{-10} s^{-1}. At low strain rates (Zener and Hollomon, 1944; Hirth and Tullis, 1992; Takahashi, 1998; Qi et al., 2017) and at high temperatures (Cross and Skemer, 2019), dynamic recrystallization and grain growth will be enhanced. The resulting CPO (Fig. 10b) will thus likely reflect a small part of the deformational history and have been continually reset as deformation proceeded.

7 Conclusions

By developing a new sample preparation method to create composite sections for each sample collected, we

https://doi.org/10.5194/tc-2020-135
Preprint. Discussion started: 8 June 2020

are able to use cryo-EBSD to obtain complete (c- and a-axes) crystallographic orientation measurements for interpreting CPO patterns in natural, coarse-grained glacial ice. A single composite section captures a relatively large number (~50-100) of grains, in our case from an ice sample of ~200mm x 150mm x 75mm dimensions and with >20mm grain size. The larger number of grains in this new approach allows us to better characterize CPO patterns in coarse-grained ice than has been done previously, and it sheds new light on the significance of microstructural processes associated with previously identified multi-maxima CPO patterns. Specifically, we conclude that a grain sampling bias of interlocking, large (>20mm) branched crystals that appear multiple times as apparent island grains in thin section contributes to the apparent multiple maxima CPOs displayed in our natural ice samples. Such bias also likely contributed to similar CPOs that have long been identified in other studies of natural, warm, coarse-grained ice. Without better establishing 3D grain size and shape, it will be difficult to fully eliminate or account for this bias, but a combination of systematic sampling, composite sample preparation, and data stacking will help more accurately define CPOs.

We suspect that in our study, a more representative CPO, if enough data from a large enough volume of ice were sampled, would consist of: 1) a c-axis CPO with one maximum that may be extended or "pulled apart" in a plane perpendicular to the shear direction, and a weaker maximum 45º-60º from the shear plane; and 2) a broad girdle of a-axes parallel to the shear plane with a cluster perpendicular to the shear direction. Such a pattern assumes that the dynamic recrystallization of ice under slow strain rate and high temperature conditions results in the observed large grain size and resetting of CPO to reflect the local kinematic conditions.

Our new sample preparation method allows for faster and more accurate collection of complete crystallographic orientation data and microstructural analyses of coarse-grained ice. This opens a range of opportunities for further analyses to aid in the understanding of micromechanical processes governing rheological properties of such ice. Future work will benefit from better quantification of 3D grain size and shape to help improve the sample preparation methods in order to minimize any grain sampling bias. Additionally, more work should be done to quantify the effects of dynamic recrystallization in the context of shear strain along the margins of glaciers and should be taken into account when assessing these CPO patterns.

Acknowledgements. We are grateful to the University of Stockholm and the Tarfala Research Station for making this field work possible and providing us with the tools necessary to access the glacier and collect samples, to Troy Zimmerman for his field assistance and to Hannah Blatchford for her help transporting samples to New Zealand and aiding in sample preparation. This research was made possible by funding provided by Graduate Student Research Grant administered by the Geological Society of America, and Grant-in-Aid of Research administered by Sigma Xi, the Scientific Research Society.

References

Allen, C.R., Kamb, W.B., Meier, M.F., and Sharp, R.P.: Structure of the lower Blue Glacier, Washington, J. Geol., 68, 601-625, https://doi.org/10.1086/626700, 1960.

Alley, R.B.: Fabrics in polar ice sheets; development and prediction, Science, 240, 493-495, https://doi.org/10.1126/science.240.4851.493, 1988.

Alley, R.B.: Flow-law hypothesis for ice-sheet modeling, J. Glaciol., 38, 245-256, https://doi.org/10.3189/S0022143000003658, 1992.

https://doi.org/10.5194/tc-2020-135
Preprint. Discussion started: 8 June 2020

Azuma, N., Wang, Y., Mori, K., Narita, H., Hondoh, T., Shoji, H., and Watanabe, O.: Textures and fabrics in the Dome F (Antarctica) ice core, Ann. Glaciol., 29,163-168, https://doi.org/10.3189/172756499781821148, 1999.

Azuma, N., Wang, Y., Yoshida, Y., Narita, H., Hondoh, T., Shoji, H., and Watanabe, O.: Crystallographic analysis of the Dome Fuji ice core, In: Hondoh, T. (Ed.), Physics of Ice Core Records. Hokkaido University Press, Sapporo, 45-61, 2000.

Bachmann, F., Hielscher, R., and Schaeben, H.: Texture Analysis with MTEX–Free and Open Source Software Toolbox, Solid State Phenomena, 160, 63-68. https://doi.org/10.4028/www.scientific.net/SSP.160.63, 2010.

Bamber, J. L., Oppenheimer, M., Kopp, R. E., Aspinall, W. P., and Cooke, R. M.: Ice sheet contributions to future sea-level rise from structured expert judgment, Proceedings of the National Academy of Sciences of the United States of America, 116 (23),11195-11200, https://doi.org/10.1073/pnas.1817205116, 2019.

Bindschadler, R. A., Nowicki, S., Abe-Ouchi, A., Aschwanden, A., Choi, H., Fastook, J., Granzow, G., Greve, R., Gutowski, G., Herzfeld, U., Jackson, C., Johnson, J., Khroulev, C., Levermann, A., Lipscomb, W. H., Martin, M. A., Morlighem, M., Parizek, B. R., Pollard, D., Price, S. F., Ren, D. D., Saito, F., Sato, T., Seddik, H., Seroussi, H., Takahashi, K., Walker, R., and Wang, W. L.: Ice-sheet model sensitivities to environmental forcing and their use in projecting future sea level (the SeaRISE project), J. Glaciol., 59 (214), 195-224, https://doi.org/10.3189/2013JoG12J125, 2013.

Bons, P.D., Kleiner, T., Llorens, M.-G., Prior, D.J., Sachau, T., Weikusat, I., and Jansen, D.: Greenland Ice Sheet: higher nonlinearity of ice flow significantly reduces estimated basal motion, Geophys. Res., 45(13), 6542-6548, https://doi.org/10.1029/2018GL078356, 2018.

Bouchez, J. L. and Duval, P.: The fabric of polycrystalline ice deformed in simple shear: experiments in torsion, natural deformation and geometrical interpretation, Texture Microstruct., 5, 171–190, https://doi.org/10.1155/TSM.5.171, 1982.

Budd, W.F.: The development of crystal orientation fabrics in moving ice, Z. Gletscherkd. Glazialgeol. 8, 65-105, https://doi.org/10.1029/2003JB002425, 1972.

Budd, W.F., and Jacka, T.H.: A review of ice rheology for ice sheet modeling, Cold Reg. Sci. Technol., 16, 107–144, https://doi.org/10.1016/0165-232X(89)90014-1, 1989.

Budd, W. F., Warner, R. C., Jacka, T. H., Li, J., and Treverrow, A.: Ice flow relations for stress and strain-rate components from combined shear and compression laboratory experiments, J. Glaciol., 59, 374–392, https://doi.org/10.3189/2013JoG12J106, 2013.

Craw, L., Qi, C., Prior, D.J., Goldsby, D.L., and Kim, D.: Mechanics and microstructure of deformed natural anisotropic ice, J. Struct. Geol., 115, 152-166, https://doi.org/10.1016/j.jsg.2018.07.014, 2018.

Cross, A. J., and Skemer, P.: Rates of dynamic recrystallization in geologic materials, J. Geophys. Res., Solid Earth 124 (2), 1324-1342, https://doi.org/10.1029/2018JB016201, 2019.

Cuffey, K.M., and Paterson, W.S.B.: The Physics of Glaciers. Elsevier, Amsterdam, Netherlands (NLD), 2010.

Dempsey, D.E., and Langhorne, P.J.: Geometric properties of platelet ice crystals, Cold Regions Science and Technology, 78, 1-13, https://doi.org/10.1016/j.coldregions.2012.03.002, 2012.

Dingley, D. J.: Diffraction from Sub-Micron Areas Using Electron Backscattering in a Scanning Electron-Microscope, Scanning Electron Microscopy, Part 2, 569-575, 1984.

https://doi.org/10.5194/tc-2020-135
Preprint. Discussion started: 8 June 2020

Durand, G., Svensson, A., Persson, A., Gagliardini, O., Gillet-Chaulet, F., Sjolte, J., Montagnat, M., and Dahl-Jensen, D.: Evolution of the texture along the EPICA Dome C Ice Core, Low Temp. Sci. 68, 91-105, http://hdl.handle.net/2115/45436, 2009.

Dutton, A., Carlson, A. E., Long, A. J., Milne, G. A., Clark, P. U., DeConto, R., Horton, B. P., Rahmstorf, S., and Raymo, M. E.: Sea-level rise due to polar ice-sheet mass loss during past warm periods, Science, 349 (6244), 10.1126/science.aaa4019, 2015.

Duval, P.: Creep and fabrics of polycrystalline ice under shear and compression, J. Glaciol., 27, 129-140, https://doi.org/10.3189/S002214300001128X, 1981.

Duval, P., Ashby, M.F., and Anderman, I.: Rate-controlling processes in the creep of polycrystalline ice, J. Phys. Chem., 87, 4066-4074, https://doi.org/10.1021/j100244a014, 1983.

Duval, P., and Castelnau, O.: Dynamic recrystallization of ice in polar ice sheets, Journal De Physique Iv, 5(C3), 197-205, https://doi.org/10.1051/jp4:1995317, 1995.

EPICA Community Members: Eight glacial cycles from an Antarctic ice core, Nature, 429 (6992), 623-628, https://doi.org/10.1038/nature02599, 2004.

Faria, S.H., Weikusat, I., and Azuma, N.: The microstructure of polar ice. Part I: Highlights from ice core research, J. Struct. Geol., 61, 2-20, https://doi.org/10.1016/j.jsg.2013.09.010, 2014.

Faria, S.H., Weikusat, I., and Azuma, N.: The microstructure of polar ice. Part II: State of the art, J. Struct. Geol., 61, 21-49, https://doi.org/10.1016/j.jsg.2013.11.003, 2014.

Flowers, G.E.: Glacier hydromechanics: early insights and the lasting legacy of three works by Iken and Colleagues, J. Glaciol., 56, 1069-1078, https://doi.org/10.3189/002214311796406103, 2010.

Glen, J. W.: The creep of polycrystalline ice, Proceedings of the Royal Society of London, Ser. A, 228 (1175), 519–538, https://doi.org/10.1098/rspa.1955.0066, 1955.

Golledge, N. R., Kowalewski, D. E., Naish, T. R., Levy, R. H., Fogwill, C. J., and Gasson, E. G. W.: The multi-millennial Antarctic commitment to future sea-level rise, Nature, 526 (7573), 421-425, https://doi.org/10.1038/nature15706, 2015.

Goossens, T., Sapart, C. J., Dahl-Jensen, D., Popp, T., El Amri, S., and Tison, J. L.: A comprehensive interpretation of the NEEM basal ice build-up using a multi-parametric approach, The Cryosphere, 10(2), 553-567, https://doi.org/10.5194/tc-10-553-2016, 2016.

Gow, A.J., and Meese, D.A.: Physical properties, crystalline textures and c-axis fabrics of the Siple Dome (Antarctica) ice core, J. Glaciol., 53 (183), 573-584, https://doi.org/10.3189/002214307784409252, 2007.

Gow, A.J., Meese, D.A., Alley, R.B., Fitzpatrick, J.J., Anandakrishnan, S., Woods, G.A., and Elder, B.C.: Physical and structural properties of the Greenland ice sheet project 2 ice core: a review, J. Geophys. Res., 102, 26559-26575, https://doi.org/10.1029/97JC00165, 1997.

Gow, A.J., and Williamson, T.: Rheological implications of the internal structure and crystal fabrics of the West Antarctic ice sheet as revealed by deep core drilling at Byrd Station, Geol. Soc. Am. Bull., 87, 1665-1677, https://doi.org/10.1130/0016-7606(1976)87<1665:RIOTIS>2.0.CO;2, 1976.

Hambrey, M.J.: The origin of foliation in glaciers; evidence from some Norwegian examples, J. Glaciol., 14, 181-185, https://doi.org/10.3189/S0022143000013496, 1975.

Hambrey, M.J., and Milnes, A.G.: Structural geology of an alpine glacier (Griesgletscher, Valais, Switzerland), Eclogae Geologicae Helvetiae, 70, 667-684, https://doi.org/10.3189/S0022143000010455, 1977.

https://doi.org/10.5194/tc-2020-135
Preprint. Discussion started: 8 June 2020

Hambrey, M.J., Milnes, A.G., and Siegenthaler, H.: Dynamics and structure of Griesgletscher, Switzerland, J. Glaciol., 25, 215-228, https://doi.org/10.3189/S0022143000010455, 1980.

Hanson, B.: A fully three-dimensional finite-element model applied to velocities on Storglaciären, Sweden, J. Glaciol., 41, 91-102, https://doi.org/10.3189/S0022143000017792 , 1995.

Herron, S.L., and Langway, Jr., C.C.: A comparison of ice fabrics and textures at Camp Century, Greenland and Byrd Station, Antarctica, Ann. Glaciol., 3, 118-124, https://doi.org/10.3189/S0260305500002639, 1982.

Herron, S.L., Langway, Jr., C.C., and Brugger, K.A.: Ultrasonic velocities and crystalline anisotropy in the ice core from Dye 3, Greenland. In: Langway Jr., C.C., Oeschger, H., Dansgaard, W. (Eds.), Greenland Ice Core: Geophysics, Geochemistry, and the Environment, Geophys. Monograph, vol. 33. American Geophysical Union, Washington, DC, pp. 23-31, https://doi.org/10.1029/GM033p0023, 1985.

Hirth, G., and Tullis, J.: Dislocation Creep Regimes in Quartz Aggregates, J. Struct. Geol., 14(2), 145-159, https://doi.org/10.1016/0191-8141(92)90053-Y, 1992.

Holmlund, P., and Eriksson, M.: The cold surface layer on Storglaciären, Geogr. Ann., 71A(3/4), 241-244, https://doi.org/10.2307/521394, 1989.

Holmlund, P., Näslund, J.O., and Richardson, C.: Radar surveys on Scandinavian glaciers, in search of useful climate archives, Geogr. Ann., 78A(2/3), 147-154, https://doi.org/10.1080/04353676.1996.11880460, 1996.

Hooke, R.L., Brzozowski, J., and Bronge, C.: Seasonal variations in surface velocity, Storglaciären, Sweden, Geografiska Annaler, 65A, 263-277, https://doi.org/10.1080/04353676.1983.11880091, 1983b.

Hooke, R.L., Calla, P., Holmlund, P., Nilsson, M., and Stroeven, A.: A 3 year record of seasonal variations in surface velocity, Storglaciären, Sweden, J. Glaciol., 35, 235-247, https://doi.org/10.3189/S0022143000004561, 1989.

Hooke, R. LeB., Gould, J.E., and Brzozowski, J.: Near-surface temperatures near and below the equilibrium line on polar and subpolar glaciers, Z. Gletscherkd. Glazialgeol, 19(1), 1-25, 1983a.

Hooke, R. LeB., and Hudleston, P.J:. Origin of foliation in glaciers, J. Glaciol., 20, 285-299, https://doi.org/10.3189/S0022143000013848, 1978.

Hooke, R. LeB., and Hudleston, P.J.: Ice fabrics from a borehole at the top of south dome, Barnes Ice Cap, Baffin Island, Geol. Soc. Am. Bull., 92, 274-281, https://doi.org/10.1130/0016-7606(1981)92<274:IFFABA>2.0.CO;2, 1981.

Hudleston, P.J.: Progressive deformation and development of fabric across zones of shear in glacial ice, In: Saxena, S., Bhattacharji, S. (Eds.), Energetics of Geological Processes. Springer, Verlag, New York, 121-150, https://doi.org/10.1007/978-3-642-86574-9_7, 1977a.

Hudleston, P.J.: Structures and fabrics in glacial ice: A review, J. Struct. Geol., 81, 1-27, https://doi.org/10.1016/j.jsg.2015.09.003, 2015.

Iliescu, D., Baker, I., and Chang, H.: Determining the orientations of ice crystals using electron backscatter patterns, Microscopy Research and Technique, 63(4), 183-187, https://doi.org/10.1002/jemt.20029, 2004.

Jacka, T., and Maccagnan, M.: Ice crystallographic and strain rate changes with strain in compression and extension, Cold Reg. Sci. Technol., 8(3), 269–286, https://doi.org/10.1016/0165-232X(84)90058-2, 1984.

Jacka, T. H., and Jun, L.: Flow rates and crystal orientation fabrics in compression of polycrystalline ice at low temperatures and stresses, Physics Ice Core Records, edited by T. Hondoh, pp. 83–102, Hokkaido Univ. Press, Sopporo, 2000.

https://doi.org/10.5194/tc-2020-135
Preprint. Discussion started: 8 June 2020

Jackson, M., and Kamb, B.: The marginal shear stress of Ice Stream B, West Antarctica, J. Glaciol., 43(145), 415-426, https://doi.org/10.3189/S0022143000035000, 1997.

Jennings, S.J.A., Hambrey, M.J., and Glasser, N.F.: Ice flow-unit influence on glacier structure, debris entrainment and transport, Earth Surf. Process. Landf., 39, 1279-1292, https://doi.org/10.1002/esp.3521, 2014.

Jonsson, S.: Structural studies of subpolar glacier ice, Geografiska Annaler: Series A, Physical Geography, 52,, 129-145, https://doi.org/10.1080/04353676.1970.11879818, 1970

Journaux, B., Chauve, T., Montagnat, M., Tommasi, A., Barou, F., Mainprice, D., and Gest, L.: Recrystallization processes, microstructure and crystallographic preferred orientation evolution in polycrystalline ice during high-temperature simple shear, The Cryosphere, 13 (5), 1495-1511, https://doi.org/10.5194/tc-13-1495-2019, 2019.

Kamb, W. B.: Ice petrofabric observations from Blue Glacier, Washington, in relation to theory and experiment, J. Geophys. Res., 64, 1891-1909, https://doi.org/10.1029/JZ064i011p01891, 1959.

Kamb, W. B.: Experimental recrystallization of ice under stress, in: Flow and Fracture of Rocks, edited by Heard, H. C., Borg, I. Y., Carter, N. L., and Rayleigh, C. B., American Geophysical Union, 211–242, 1972.

Langway, C.C. Jr.: Ice fabric and the universal stage, Technical Report 62, U.S. Army Snow Ice and Permafrost Research Establishment, Wilmette, Illinois, 1958.

Langway Jr., C.C., Shoji, H., and Azuma, N.: Crystal size and orientation patterns in the Wisconsin-age ice from Dye 3, Greenland, Ann. Glaciol., 10, 109-115, https://doi.org/10.3189/S0260305500004262, 1988.

Li, J., Jacka, T. H., and Budd, W. F.: Strong single-maximum crystal fabrics developed in ice undergoing shear with unconstrained normal deformation, Ann. Glaciol., 30, 88–92, https://doi.org/10.3189/172756400781820615, 2000.

Lile, R.C.: The flow law for isotropic and anisotropic ice at low strain rates, ANARE Reports, 132, 93, 1984.

Lipenkov, V.Y., Barkov, N.I., Duval, P., and Pimienta, P.: Crystalline texture of the 2083 m ice core at Vostok Station, Antarctica, J. Glaciol., 35 (121), 392-398, https://doi.org/10.3189/S0022143000009321, 1989.

MacGregor, J. A., Fahnestock, M. A., Catania, G. A., Aschwanden, A., Clow, G. D., Colgan, W. T., Gogineni, P.S., Morlighem, M., Nowicki, S.M.J., Paden, J.D., Price, S. and F., Seroussi, H.: A synthesis of the basal thermal state of the Greenland Ice Sheet, J. Geophys. Res., Earth Surface, 121, 1328–1350. https://doi.org/10.1002/2015JF003803, 2016.

Mainprice, D., Bachmann, F., Hielscher, and R., Schaeben, H.: Descriptive tools for the analysis of texture projects with large datasets using MTEX: strength, symmetry and components, Geol. Soc. Lond. Spec. Publ., 409, 251–271, http://dx.doi.org/10.1144/SP409.8, 2015.

Matsuda, K.: Determination of a-axis orientations of pollycrystalline ice, J. Glaciol., 22(86), 165-169, https://doi.org/10.3189/S0022143000014143, 1979.

Matsuda, M., and Wakahama, G.: Crystallographic structure of polycrystalline ice, J. Glaciol., 21, 607-620, https://doi.org/10.3189/S0022143000033724, 1978.

Miyamoto, A., Weikusat, I., and Hondoh, T.: Complete determination of ice crystal orientation using Laue X-ray diffraction method, J. Glaciol., 57(201), 103-110, https://doi.org/10.3189/002214311795306754, 2011.

Montagnat, M., Chauve, T., Barou, F., Tommasi, A., Beausir, B., and Fressengeas, C.: Analysis of dynamic recrystallization of ice from EBSD orientation mapping, Front. Earth Sci., 3, 81, https://doi.org/10.3389/feart.2015.00081, 2015.

https://doi.org/10.5194/tc-2020-135
Preprint. Discussion started: 8 June 2020

Montagnat, M., Azuma, N., Dahl-Jensen, D., Eichler, J., Fujita, S., Gillet-Chaulet, F., Kipfstuhl, S., Samyn, D., Svensson, A., and Weikusat, I.: Fabric along the NEEM ice core, Greenland, and its comparison with GRIP and NGRIP ice cores, The Cryosphere, 8 (4), 1129-1138, https://doi.org/10.5194/tc-8-1129-2014, 2014.

Pauling, L.: The structure and entropy of ice and other crystals with some randomness of atomic arrangement, J. Am. Chem. Soc., 57, 2680-2684, https://doi.org/10.1021/ja01315a102, 1935.

Pearce, M.A.: EBSDinterp 1.0 : a MATLAB ® program to perform microstructurally constrained interpolation of EBSD data, Microsc. Microanal., 21, 985–993, https://doi.org/10.1017/S1431927615000781, 2015.

Pettersson, R., Jansson, P., and Holmlund, P.: Cold surface layer thinning on Storglaciären, Sweden, observed by repeated ground penetrating radar surveys, J. Geophys. Res., 108(F1), 6004, https://doi.org/10.1029/2003JF000024, 2003.

Pettersson, R., Jansson, P., Huwald, H., and Blatter, H.: Spatial pattern and stability of the cold surface layer of Storglaciären, Sweden, J. Glaciol., 53, 99-109, https://doi.org/10.3189/172756507781833974, 2007.

Piazolo, S., Wilson, C. J., Luzin, V., Brouzet, C., and Peternell, M.: Dynamics of ice mass deformation: Linking processes to rheology, texture, and microstructure, Geochem. Geophys. Geosyst., 14(10), 4185–4194, https://doi.org/10.1002/ggge.20246, 2013.

Prior, D. J., Boyle, A. P., Brenker, F., Cheadle, M. C., Day, A., Lopez, G., Peruzzo, L., Potts, G. J., Reddy, S., Spiess, R., Timms, N. E., Trimby, P., Wheeler, J., and Zetterstrom, L.: The application of electron backscatter diffraction and orientation contrast imaging in the SEM to textural problems in rocks, American Mineralogist, 84 (11-12), 1741-1759, https://doi.org/10.2138/am-1999-11-1204, 1999.

Prior, D.J., Lilly, K., Seidemann, M., Vaughan, M., Becroft, L., Easingwood, R., Diebold, S., Obbard, R., Daghlian, C., Baker, I., Caswell, T., Golding, N., Goldsby, D., Durham, W.B., Piazolo, S., and Wilson, C.J.L.: Making EBSD on water ice routine, J. Microsc., 259, 237-256, https://doi.org/10.1111/jmi.12258, 2015.

Qi, C., Goldsby, D.L., and Prior, D.J.: The down-stress transition from cluster to cone fabrics in experimentally deformed ice, Earth Planet. Sci. Lett., 471, 136–147, https://doi.org/10.1016/j.epsl.2017.05.008, 2017.

Qi, C., Prior, D.J., Craw, L., Fan, S., Lloren, M-G., Griera, A., Negrini, M., Bons, P.B., and Goldsby, D.L.: Crystallographic preferred orientations of ice deformed in direct-shear experiments at low temperatures, The Cryosphere, 13, 351-371, https://doi.org/10.5194/tc-13-351-2019, 2019.

Ragan, D.M.: Structures at the base of an ice fall, J. Geol., 77, 647-667, http://doi.org/10.1086/627463, 1969.

Ramsay, J.G.: Folding and fracturing of rocks, McGraw Hill, New York, 1967.

Rignot, E., and Mouginot, J.: Ice flow in Greenland for the International Polar Year 2008–2009, Geophysical Research Letters, 39, L11501. https://doi.org/10.1029/2012GL051634, 2012.

Rigsby, G.P.: Crystal fabric studies on Emmons Glacier, Mount Rainer, Washington, J. Geol., 61, 482-509, https://doi.org/10.1086/625914, 1951.

Rigsby, G.P.: Crystal orientation in a glacier and in experimentally deformed ice, J. Glaciol., (3) 27, 589-606, https://doi.org/10.3189/S0022143000023716, 1960.

Roberson, S.: Structural composition and sediment transfer in a composite cirque glacier: Glacier de St. Sorlin, France, Earth Surf. Process. Landf., 33, 1931-1947, https://doi.org/10.1002/esp.1635, 2008.

Russell-Head, D. S., and Wilson, C. J. L.: Automated fabric analyser system for quartz and ice, J. Glaciol., 24, 117–130, 2001.

https://doi.org/10.5194/tc-2020-135
Preprint. Discussion started: 8 June 2020

Seddik, H., Greve, R., Placidi, L., Hamann, I., and Gagliardini, O.: Application of a continuum-mechanical model for the flow of anisotropic polar ice to the EDML core, Antarctica, J. Glaciol., 54 (187), 631-642, https://doi.org/10.3189/002214308786570755, 2008.

Schytt, V.: Snow and ice studies in Antarctica. Ph.D. Thesis, University of 1512 Stockholm, In: Norwegian–British–Swedish Antarctic Expedition, 1949–1952, 1513 Scientific Results 4, Glaciology II. Norsk Polarinstitutt, Oslo, 1958.

Steinemann, S.: Experimentelle Untersuchungen zur Plastizitat von Eis, Beitr. Geol. Schweiz, Hydrologie, 10, 46-50, https://doi.org/10.3929/ethz-a-000096707, 1958b.

Svensson, A., Schmidt, K.G., Dahl-Jensen, D., Johnsen, S.J., Wang, Y., Kipfstuhl, and J., Thorsteinsson, T.: Properties of ice crystals in NorthGRIP late- to middle- Holocene ice, Ann. Glaciol., 37, 113-118, https://doi.org/10.3189/172756403781815636, 2003b.

Takahashi, M.: Fractal analysis of experimentally, dynamically recrystallized quartz grains and its possible application as a strain rate meter, J. Struct. Geol., 20(2-3), 269-275, https://doi.org/10.1016/S0191-8141(97)00072-2, 1998.

Thorsteinsson, T., Kipfstuhl, J., and Miller, H.: Textures and fabrics in the GRIP ice core, J. Geophys. Res., 102, 26583-26599, https://doi.org/10.1029/97JC00161, 1997.

Thwaites, R. J., Wilson, C. J. L., McCray, A. P.: Relationship between bore-hole closure and crystal fabrics in Antarctic ice core from Cape Folger. J. Glaciol., 30 (105), 71-179, https://doi.org/10.3189/S0022143000005906, 1984.

Treverrow, A., Budd, W. F., Jacka, T. H., and Warner, R. C.: The tertiary creep of polycrystalline ice: Experimental evidence for stress-dependent levels of strain-rate enhancement, J. Glaciol., 58(208), 301–314, https://doi.org/10.3189/2012JoG11J149, 2012.

Urai, J. L., Means, W. D., and Lister, G. S.: Dynamic recrystallization of minerals, in: Mineral and Rock Deformation, edited by: Hobbs, B. and Heard, H., Laboratory Studies, 36, 161–199, 1986.

Van der Veen, C.J., and Whillans, I.M.: Development of fabric in ice, Cold Regions Science and Technology, 22, 171-195, https://doi.org/10.1016/0165-232X(94)90027-2, 1994.

Vaughan, M.J., Prior, D.J., Jefferd, M., Brantut, N., Mitchell, T.M., and Seidemann, M.: Insights into anisotropy development and weakening of ice from in situ P wave velocity monitoring during laboratory creep, J. Geophys. Res., Solid Earth, 122, 7076-7089. https://doi.org/10.1002/2017JB013964, 2017.

Wang, Y., Thorsteinsson, T., Kipfstuhl, J., Miller, H., Dahl-Jensen, D., and Shoji, H.: A vertical girdle fabric in the NorthGRIP deep ice core, North Greenland, Ann. Glaciol., 35, 515-520, https://doi.org/10.3189/172756402781817301, 2002.

Weertman, J.: Creep deformation of ice, Annu. Rev. Earth Planet. Sci., 11, 215-240, https://doi.org/10.1146/annurev.ea.11.050183.001243, 1983.

Weikusat, I., Jansen, D., Binder, T., Eichler, J., Faria, S. H., Wilhelms, F., Kipfstuhl, S., Sheldon, S., Miller, H., Dahl-Jensen, D., and Kleiner, T.: Physical analysis of an Antarctic ice core-towards an integration of micro- and macrodynamics of polar ice, Philosophical Transactions of the Royal Society a-Mathematical Physical and Engineering Sciences, 375 (2086), 1-27, https://doi.org/10.1098/rsta.2015.0347, 2017.

https://doi.org/10.5194/tc-2020-135
Preprint. Discussion started: 8 June 2020

Weikusat, I., Kipfstuhl, S., Faria, S.H., Azuma, N., and Miyamoto, A.: Subgrain boundaries and related microstructural features in EDML (Antarctica) deep ice core, J. Glaciol., 55(191), 461-472, https://doi.org/10.3189/002214309788816614, 2009b.

Weikusat, I., Miyamoto, A., Faria, S.H., and Kipfstuhl, S., Subgrain boundaries in Antarctic ice quantified by X-ray Laue diffraction, J. Glaciol., 57(201), 111-120, https://doi.org/10.3189/002214311795306628, 2011.

Wenk, H.R., and Christie, J.: Comments on the interpretation of deformation textures in rocks, J. Struct. Geol., 13(10), 1091-1110, https://doi.org/10.1016/0191-8141(91)90071-P, 1991.

Wilen, L.A., Diprinzio, C.L., Alley, R.B., and Azuma, N.: Development, principles, and applications of automated ice fabric analyzers, Microscopy Research and Technique, 62, 2-18, https://doi.org/10.1002/jemt.10380, 2003.

Wilson, C.J.L., Peternell, M., Hunter, N.J.R., and Luzin, V.: Deformation of polycrystalline D_2O ice: Its sensitivity to temperature and strain-rate as an analogue for terrestrial ice, Earth and Planetary Science Letters, 532 (115999), 1-15, https://*doi*.org/10.3189 /172756494587384, 2020.

Wilson, C.J.L., Peternell, M., Piazolo, S., and Luzin, V.: Microstructure and fabric development in ice: Lessons learned from *in situ* experiments and implications for understanding rock evolution, J. Struct. Geol., 61, 50-77, https://doi.org/10.1016/j.jsg.2013.05.006, 2014.

Wongpan, P., Prior, D.J., Langhorne, P.J., and Lilly, K.: Using electron backscatter diffraction to measure full crystallographic orientation in Antarctic land-fast sea ice, J. Glaciol., 64(247), https://doi.org/10.1017/jog.2018.67, 2018.

Zener, C., and Hollomon, J. H.: 1944, Effect of strain rate upon plastic flow of steel, Journal of Applied Physics, 15(1), 22-32, https://doi.org/10.1063/1.1707363, 1944.

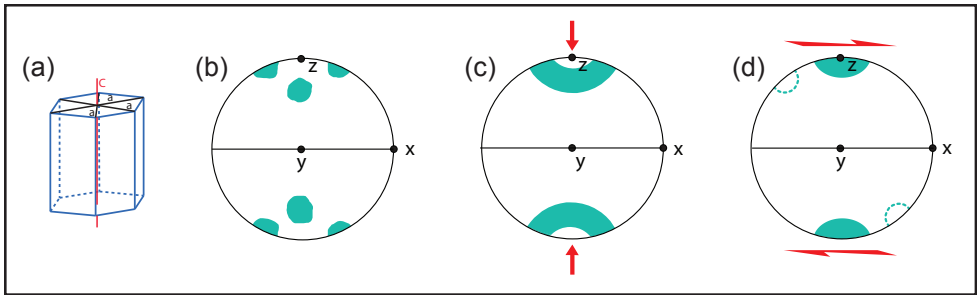

Figure 1. Schematic image showing (a) an ice crystal and its defining c- and a-axes; (b) multimaxima fabric pattern identified in warm, coarse-grained glacial ice, (c) a small circle girdle or cone shape in uniaxial compression and (d) a strong single maximum fabric ± a weaker second maximum in simple shear. (c) and (d) are from experiments and (c) (arguably) and (d) also from nature. CPO plots here and in subsequent figures are all equal-area, lower hemisphere projections. In (b) and (d), z is normal to the foliation, and x is parallel to the shear direction. There is no shear plane implied in (c).

https://doi.org/10.5194/tc-2020-135
Preprint. Discussion started: 8 June 2020

The Cryosphere
Discussions
Open Access
EGU

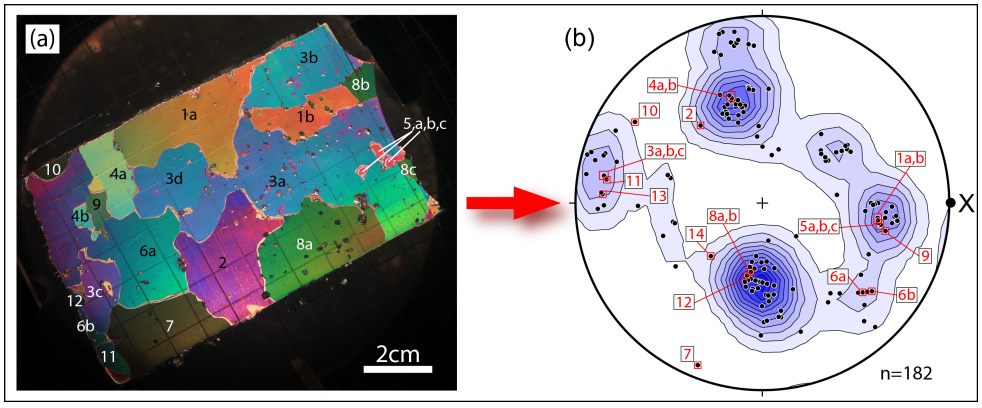

Figure 2. (a) A thin section under cross-polarized light from sample SG6-B collected in 2016. Grains are labelled based on their c-axis orientations, measured using a universal Rigsby stage. Grains with the same orientation were tentatively marked as the same grain as indicated by lettering. Color gradients across some larger grains are a result of inconsistent thin section thickness; (b) Associated c-axis plot compiled from 8 thin sections from the sample SG6-B. This plot contains orientations of all grains measured, and is contoured using the Kamb method (Kamb, 1959). When possible duplicates within the same section are removed, the pattern maintains its multimaxima nature, but is weaker (not shown). Numbered data points correspond to numbered grains in (a). In order to obtain 100 individual crystal measurements, 5-15 thin sections had to be made for each sample, depending on the overall grain size in the individual sample. The projection is plotted such that the pole to foliation is vertical and x is the flow direction.

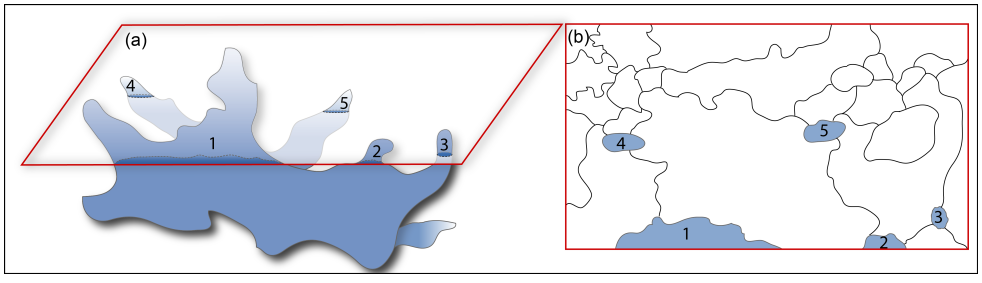

Figure 3. (a) Schematic branching crystal and associated (b) two-dimensional thin section highlighting the notion of island grains that would appear in a two-dimensional thin section. Numbered branches in three dimensions correspond to the numbered island grains in two-dimensions. Part of the grain in (a) lies above the section and part below.

https://doi.org/10.5194/tc-2020-135
Preprint. Discussion started: 8 June 2020

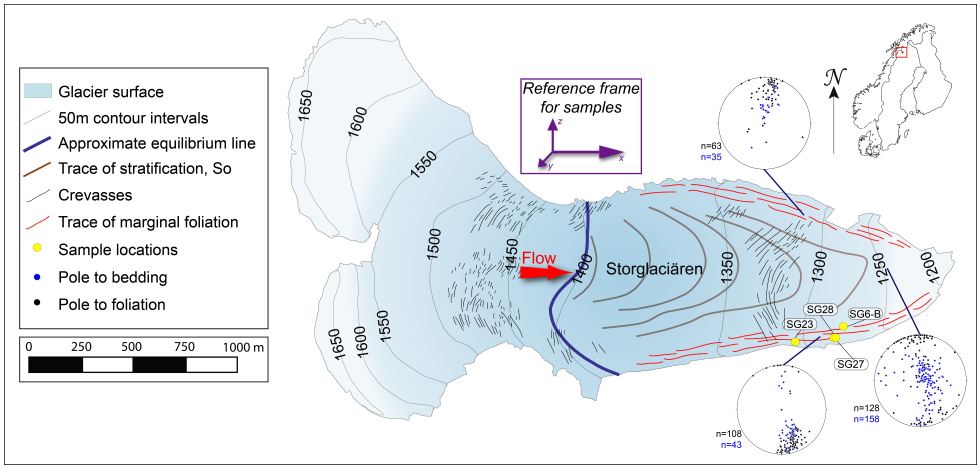

Figure 4. Simplified map of Storglaciären highlighting the traces of structural elements and orientations of foliation and bedding for the north margin, south margin, and center of the glacier in the ablation zone. Locations of samples SG6-B, SG23, SG27 and SG28 are labelled. The orientation diagrams of planar fabric elements (stratification and foliation) are in geographic coordinates. The sample reference frame for the remainder of the paper is represented, where x is the flow/shear direction y is the vorticity axis and z is north.

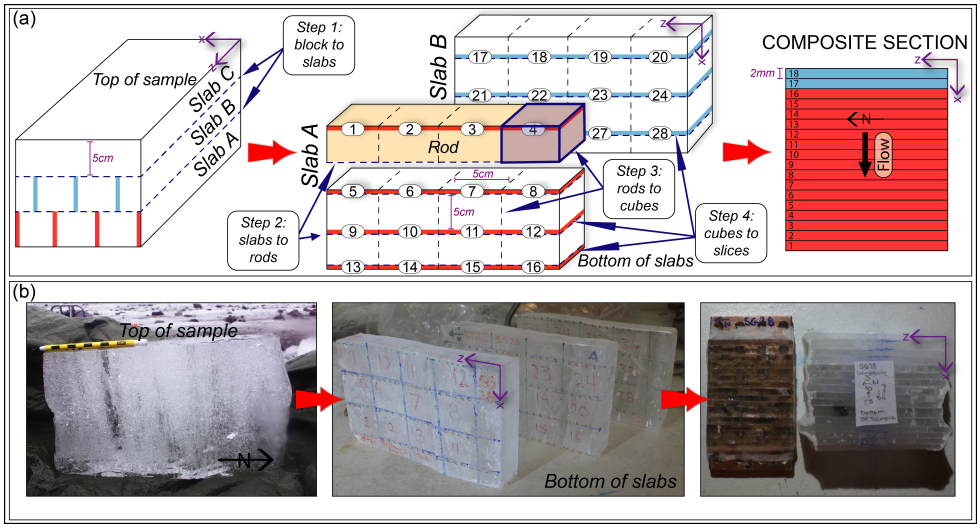

Figure 5. (a) Schematic sample preparation for one composite section. Steps for each cut to progress from sample to slice are specified with dashed lines, and examples of each are highlighted with dark blue arrows. Individual 2mm slices are shown throughout the process on slab A and slab B, and the numbers correspond to those in the unique slice in the final composite stack. At least 36 slices were cut from every sample (using slabs A, B and C) to construct composite sections. At least two composites for each sample comprised the final data set (1 composite comprised of slices 1-18 is shown in figure). (b) Sample preparation illustrated using SG28 from block sample to composite section. Note that the number sequences varied from sample to sample so the numbers on the slabs do not match the schematic in (a). Composites are oriented in a kinematic reference frame such that x is the flow/shear direction, y is the vorticity axis and z is north.

https://doi.org/10.5194/tc-2020-135
Preprint. Discussion started: 8 June 2020

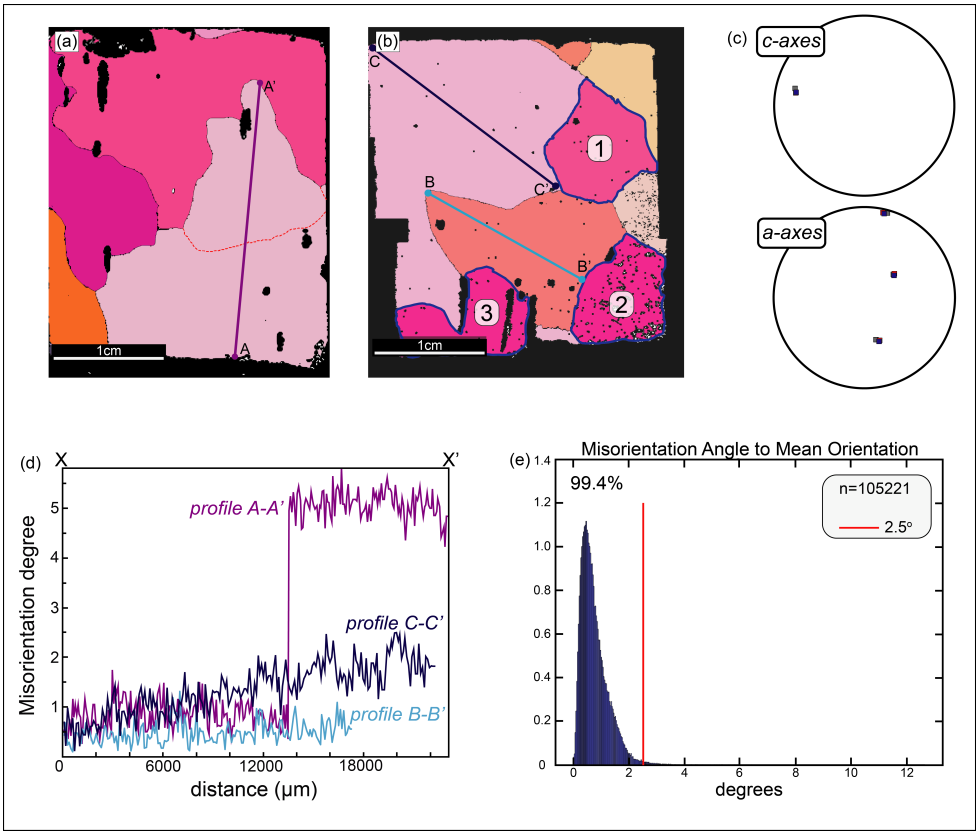

790 **Figure 6. A typical whole section EBSD analysis with: (a) and (b) maps of whole sections from SG28. (a) Subgrain boundary is shown with a red dashed line, and profile A-A' crosses that boundary, (b) highlighting three potential island grains within the section, and profile lines B-B' and C-C' across two grains; (c) one-point-per-grain c- and a-axes of the highlighted grains 1, 2 and 3 in B. (d) misorientations profiles relative to first pixel along A-A', B-B' and C-C'; (e) Misorientation angle of each pixel in EBSD map (b) with respect to the mean orientation of the grain. The red line highlights that 99.4% of the misorientations between pixels lie below 2.5°.**

https://doi.org/10.5194/tc-2020-135
Preprint. Discussion started: 8 June 2020

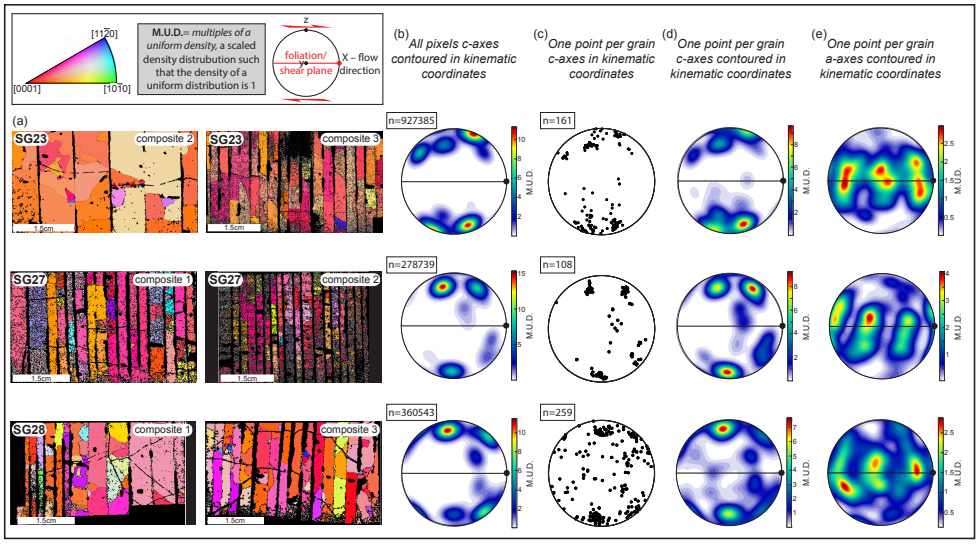

Figure 7. EBSD maps and associated CPOs for composite sections from samples SG23, SG27 and SG28. Data from each pair of composites are combined to give the bulk CPO for each sample. (a) EBSD images of the two composite sections, where the vertical black lines represent junctions between individual slices of the composite. (b) contoured plots of c-axis orientations of all pixels; (c) uncontoured plots of c-axis orientations representing one-point-per-grain; (d) contoured plots of c-axis orientations representing one-point-per-grain; and (e) contoured a-axis orientations representing one-point-per-grain. All plots are in a kinematic reference frame where x is the shear flow/shear direction (black dot), y is the vorticity axis and z is north.

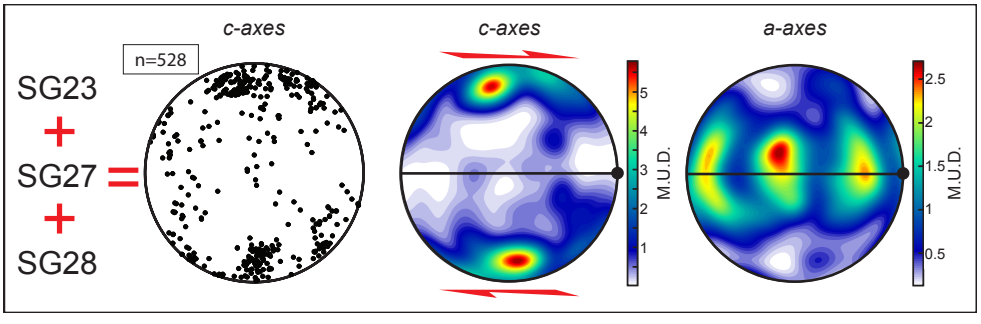

Figure 8. Combined data (one-point-per-grain) from SG23, SG27 and SG28 in the same kinematic reference frame. Plots from left to right show c-axes uncontoured, c-axes contoured and a-axes contoured.

https://doi.org/10.5194/tc-2020-135
Preprint. Discussion started: 8 June 2020

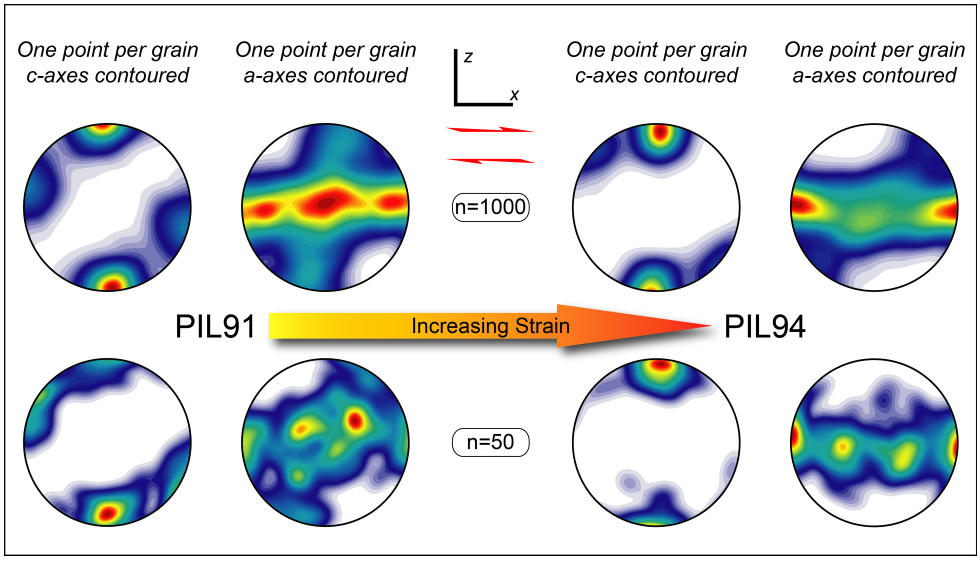

Figure 9. Samples PIL91 (γ= 0.62) and PIL94 (γ= 1.5) from Qi et al. (2019), displaying the full data set, and a typical subset of randomly resampled data. Both of these samples were deformed at -5°C at 20MPa confining pressure in a cryogenic gas medium apparatus under constant axial displacement rates and terminated at different shear strains. In all cases, the pole figures are in kinematic coordinates, with x being the shear direction and x-y the shear plane.

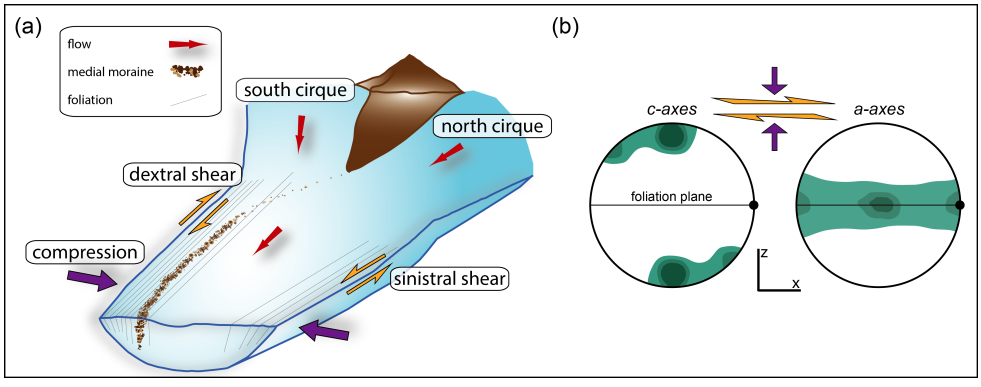

Figure 10. (a) Schematic of the combination of simple shear and compression experienced by the ice as the valley narrows (similar to Storglaciären) and (b) associated schematic CPO plots (for marginal ice) expected for dynamic recrystallization at low strain rates and high temperatures.